Modeling & Analysis of Environmental Orbit Perturbation and Budgeting Their Effect on Orbital Elements

Ali A.Khalaji, Kamran Raissi*

Department of Aerospace Engineering, Amirkabir University of Technology, Tehran, Iran

A B S T R A C T

This paper examines the impact of orbit perturbations on satellite translational dynamics, encompassing both major and minor forces. The former category includes atmospheric drag, Earth oblateness, solar radiation, and third-body attractions. Atmospheric drag is based on a solar activity model and its rotation due to meridional and zonal winds. Earth oblateness is considered over a high order of Earth gravity harmonics, along with direct solar radiation pressure and the effect of third-body attraction, such as the Moon and Sun gravity, utilizing high-accuracy ephemeris. Minor force effects include Earth's solid tides resulting from the Sun and Moon attraction, the effect of reflected solar radiation pressure from the Earth (Albedo), and relativity effects. The three primary theories employed to expand equations are perturbed potential function, force components, and acceleration. An investigative study was conducted to analyze the budget of perturbations in orbital elements at various altitudes. This approach is applicable to high orbit injection, orbit transfer using low electrical propulsion, and high-precision missions. The research underscores the significance of possessing a precise perturbed dynamic model, which facilitates high-revolution orbit transfer.

KEYWORDS

Orbit Perturbations -Satellites Dynamics- Orbital elements- Orbit transfer

*Corresponding author's email: k_raissi@aut.ac.ir

1. Introduction

The unusual variations in orbital elements due to perturbations and satellite orbit cause different effects of orbital disturbances. The perturbed forces can be analyzed from different standpoints, such as considering conservative and non-conservative forces. During years, researchers have studied different models based on various functions of perturbations. Aerodynamic drag effect has been studied on the satellite lifetime based on a simple atmospheric model considering density changes with altitude, solar periodic activities as well as Earth oblateness. Results of the models have been compared with actual samples. [1], based on MSISE90, MSISE77, DTM77, J71 density model, presented a model for estimating the satellite lifetime and satellite impact point then tendered the accuracy of the model by comparing the results with the data of some low-altitude satellite. [2] studied the drag effect of atmosphere on NIMOSA satellite's perturbed acceleration and analyzed the satellite's lifetime based on changes in Ω and ω. [3] studied the drag effect with two density models, JR71 and MSISE-90 and the changes in solar intensity on 11 spherical satellites among which five satellites were below 400km, two 500 km satellite and three of them were between 750 to 850 km and one of them is about 1500 km. Based on the analysis, the MSIS-90 model is acceptable and proper model for up to 800km height. Regarding the atmosphere rotation and atmosphere oblateness, [4], studied and analyzed the drag effect for Indian RS-7 satellite and [5] on the secular decay of the LARES semi-major axis too. These effects were used by incorporating the gravitational oblateness model of the Earth up to J6 with motion equation method of KS [6]. It should be noted that significant research activities have been carried out to improve the analytical solution of the drag effect [7]. In a recent article analyzing the effect of the atmosphere on orbital parameters, no emphasis was placed on the impacts of solar activity variations, existing models, changes in the drag coefficient, atmospheric rotation, or zonal and meridional winds, nor was the flight angle addressed [8]. As being specified, the analysis of atmosphere effect was done based on NRLMSIS-00 density model with various solar activity index, drag coefficient variation and the effects of rotational atmosphere and also the zonal and meridional winds were considered.

Many have studied the effect of direct solar radiation pressure and presented various models so far. Some of these models are analytical and some are developed based on empirical models based on the observed data of satellites. [9], presented a model for studying the secular and short periodic effects of solar radiation pressure on spherical satellite based on Lagrange perturbation equations and got the normal forces and also reflected radiation from the Earth and considered the shadow model based on [10] suggestion and as a result, presenting other models like the accurate analytical model of SRP for GNSS, which was presented by [11] and is based upon simulating the solar photon flux with a pixel array. In addition, some empirical models were presented that addressing the model presented by [12], which is a new empirical model for GPS satellites. Based on the data of these satellites in interval of 4.5 years and after analysis, it was shown in these studies that this model, still being improved [13], can function up to 85% better than the best models. This effect is more significant in higher orbit objects, mainly including GEO satellites, spacecrafts, debris and space asteroids [14]. In this study, the analysis of the SRP effect based on the suggested source model [9] by Earth's shadow has been done.

Scientists extensively studied the effect of Earth's gravitational field model and developed it based on the Earth's harmonic. They extended these coefficients up to high order through satellite observations. However, in analytical study, the effect of high order harmonics has more important because the effect of J_2 is about 400 times greater than other zonal coefficients. Many researchers conducted analyses on the perturbed effects due to Earth oblateness, which we can be found in works such as [15-19]. They focused on the effects of J_2, and someone such as [20] and [21] developed this effect up to J6 and J8. In this study, perturbed acceleration on polar coordinate viewpoint is used to analyze the effect, and only the effect of zonal harmonic developed up to the order of 10 based on Legendre polynomial and generalization of it in an analytical way, and analyzed based on Gauss equation. [22] and [23] both found that this effect plays a crucial role in mission analysis accuracy and equipment calibration, respectively, such as determining the velocity of a planet's surface from orbital survey images captured by onboard cameras.

Many researchers have studied how gravitational force affects the direction of spacecraft and suggested different models. [24] attempted to produce long and short periodic components of the gravitational potential. Also, [25] evaluated the perturbed effect of attraction using classic mechanics and secular terms. Other studies such as, [26-33] used perturbed equations, potential functions and numerical methods to estimate this effect. Investigating the long-term effects of third-body attraction on a satellite around an oblate body for a high order expansion of disturbing function was done by [33]. Also [35] studied on satellite formations which were perturbed by lunar gravity to describe the relative motions and in designing frozen orbits. Recent studies have explored the gravitational perturbations induced by a third body, with particular emphasis on its orbital

*Corresponding author's email: k_raissi@aut.ac.ir

inclination and eccentricity. While these investigations have examined variations in orbital dynamics and evaluated system sensitivity with respect to mentioned parameters, a comprehensive analysis of the underlying mathematical models remains lacking [36] and [37].

The effects of small forces are frequently neglected in the comprehensive study of perturbations on satellite translational dynamics because they are of low order. They involve the effect of Earth's solid tides created by the gravity of the Sun and Moon, oceanic tides, general relativity effect, the impact of indirect solar radiation from the Earth (Albedo), and Yarkovsky effect. [38], [39], [40] and [41] presented the effect of Earth solid tides due to Sun and Moon gravity and the proper potential function for production. In addition, accurate analysis on Earth's tides effect was done by [42] on LARES satellite.

Einstein's discoveries have resulted in many attempts to expand the effect of the theory of general relativity on satellite motion equations, which were established using Newton's classical theory. Among these activities, [43] worked on a comparison of Newton and general relativity model in the motion of a particle in a gravitational field. [44] suggested the model of relativity equations of motion for Earth's orbits. [45] created the perturbed potential function and used Lagrange perturbed equations to establish the connection between changes in orbital elements over time. Additionally, recent activities, such as [46] and [47]'s actions, have had an impact on LEO and GPS satellites. In three distinct ways, relativity influenced the satellites in the equation of motion, signal propagation, and beat rate of the clocks.

Scientists have carried out thorough investigations on the Yarkovsky force, a phenomenon that causes heat drag and influences asteroids and meteoroids. Also, [48] provides non-linear theory for coplanar cases and Yarkovsky diurnal effect on metric asteroids, while [49] studied the effect of Yarkovsky heat forces on the dynamics of asteroids and [50] presented an accurate model for Yarkovsky effect. In a recent study, [51] analyzed the orbital dynamics of asteroid (101955) Bennu, considering Yarkovsky and SRP effects. [52]'s investigation focused on an asteroid's movement under the Sun's gravity and perturbing acceleration. [53] aimed to explain this effect by analyzing the asteroid's radius and velocity vector.

A review of existing literature reveals that most studies analyze only one or two perturbation effects, typically limited to specific models. The novelty of this research lies in its comprehensive approach, which integrates all perturbation effects (both major and minor) through diverse equation frameworks. Furthermore, it quantifies each perturbation's contribution and examines its variation with orbital altitude, a critical gap in current literature. Consequently, this study establishes a foundational reference for orbital mechanics practitioners, particularly in high-precision mission design.

Long-duration, high-accuracy mission such as geostationary satellite station-keeping, constellation maintenance, and long-duration orbital transfers require rigorous analysis of minor perturbations. This need becomes particularly significant in low-thrust electric propulsion systems, where multi-revolution, long-duration transfers amplify the influence of perturbations.

2. Atmosphere Drag

Atmospheric drag plays a significant role in the lifetime of a satellite, which can be extended by raising its altitude. This factor is particularly crucial, below 600 km. Due to the non-conservative force, the energy of the orbit decreases, leading to a decrease in the semi-major axis and eccentricity. The work done by drag on orbit is

$$\dot{E} = F_{Drag}.V = \left(-\frac{1}{2}\rho v^3 S C_d\right) = \frac{d}{dt}\left(-\frac{\mu}{2a}\right) \tag{1}$$

$$\dot{a} = -\frac{\rho S C_d a^2 v^3}{\mu} \tag{2}$$

The effect of drag, based on an exponential density model, is studied by [54]. Nevertheless, changes in latitude and longitude are the most important factors affecting the trend of density changes. The maximum density occurs at approximately 2pm local time, while the minimum density occurs at roughly 4am local time, as indicated by the contour of density change. Variance angle from the center of daytime bulge is the primary determinant of density. According to the [54], we have

$$\rho = \rho_0\left(1 + F\cos\phi\right)\exp\left(-\frac{r - r_0}{H}\right) \tag{3}$$

The solar flux index changes during the day and night, depending on height, season, and year variation. It has a range of 60 to 250 in the unit of $10^{-22}\mathrm{Wm}^{-2}\mathrm{Hz}^{-1}$ and is expressed as maximum and minimum.

$$\frac{\rho_{\max}}{\rho_{\min}} = \frac{1+F}{1-F} \tag{4}$$

The angular deviation of the satellite position to the day time bulge is ϕ, and [54] has explained the details about it in formula (3). φ_0 is the density for $\phi = 90^{\circ}$ in r_0 in which often the initial position is perigee and r is the instantaneous position of the satellite. We can analyze the effect of density in the Gaussian equations and components of the force, which influences along the velocity vector in the opposite direction that we can

consider as f_T and the effect of the Lift could be considered as f_N.

$$f_T = -\frac{D}{m} = -\frac{1}{2}\rho V^2 \frac{SC_D}{m} \tag{5}$$

The above equation showcases V is the satellite's velocity relative to the air and its orbit to Earth's center. However atmospheric rotation's impact is also important. In fact V is

$$V = v - V_A \quad ; \quad V_A = r\omega\cos\varphi \tag{6}$$

Where ω represents the angular velocity of the atmosphere relative to the Earth's axis, φ denotes the geocentric latitude, and v corresponds to the satellite's velocity vector. By reducing the complexity based on the relationship of parameters in the formed spherical triangle between satellites, also $u = w + \varphi$ and neglecting small terms like as r^2w^2 respect to V^2

$$V^2 = v^2\left(1 - \frac{r_p w}{v_p}\cos i\right)^2 = v^2 F \tag{7}$$

Therefore, the connection between drag and satellite velocity in relation to inertia can be expressed as:

$$D = \frac{1}{2}\rho v^2 F S C_D \tag{8}$$

Another significant point for analyzing the drag effect considered in this paper is the inequality of drag force vector with the radial component. The velocity vector of the satellite has a flight angle ψ to the radial direction, so the Gauss equations define the relationship between f_T and f_N force components based on the flight angle ψ and true anomaly θ, which can be expressed as follows:

$$f_t = \frac{1}{v}\left(\frac{\mu}{P}\right)^{1/2}\{f_T(1 + e\cos\theta) + f_N e\sin\theta\} \tag{9}$$

$$f_r = \frac{1}{v}\left(\frac{\mu}{P}\right)^{1/2}\{f_T e\sin\theta - f_N(1 + e\cos\theta)\} \tag{10}$$

The effect of aerodynamic normal force (f_n) on the orbital plane can be examined by analyzing the rotation of the atmosphere and meridional winds. Since v is in orbital plane and V_A makes an angle such as γ' with the orbital plane, the vertical component of Vcould be considered as:

$$V_n = V_A \sin\gamma' = rw\cos\phi\sin\gamma' \tag{11}$$

And by using the trigonometric relations,

$$V_n = rw\sin i\cos u \tag{12}$$

And the result will be,

$$f_n = -\frac{\rho v\delta}{2\sqrt{F}} rw\sin i\cos u \tag{13}$$

To analyze the effects of meridional wind, assume that the vector V_A will make an angle like α in respect of West–East line. So the velocity of the meridional wind $V_A\text{Sin}\alpha$ after simplifying and its correlation with the inertial speed and orbital elements is:

$$f_n = -\frac{\rho v\delta}{2\sqrt{F}}\left\{rw\sin i\cos u - \frac{r\Phi\cos i}{\left(1 - \sin^2 i\sin^2 u\right)^{1/2}}\right\} \tag{14}$$

The formula (14) is the result of perpendicular force caused by zonal and meridional winds and ϕ implies the meridional wind's angular rate. The speed of atmospheric wind is roughly $500\ \text{ms}^{-1}$ estimated based on experimental data, while the speed of meridional winds is estimated to less than $100\ \text{ms}^{-1}$.

3. Direct solar radiation pressure

Solar radiation pressure can cause a force on the satellite surface that is proportional to,

$$\vec{F}_{SR} = P_{SR} A C_P \quad ; \quad \text{P}_{\text{SR}} = 4.51\times10^{-6} \ \frac{N}{m^2} \tag{15}$$

The number of C_P absorbent and reflective objects can be anywhere from 0 to 2 and A is perpendicular plane of the satellite to the sun. Often, the effects of radiation for orbits with high altitude are very important. The relative position of the Sun, satellite and the Earth in various instances which leads to shadow effects, has striking and remarkable influences. Different models have been developed to analyze the solar radiation impact that all of them were based on force component and the only difference is modeling of eclipse influence.

The structure of equations in some phrasings includes the analytical effect of shadows, with the main body of the equation expressing the two real anomaly entrance and exit angles of the satellite as it enters and exits the shadow of the Earth, as found in [55]. Nonetheless, according to another model used to analyze this disturbance effect [56], it is assumed that the shadow of the Earth is cylindrical and by checking the position of the Sun and the satellite's entrance and exit angles instantaneously, the value of F_{SR} will be zero during the shadow interval.

$$\dot{a} = 2na^3\left(1 - e^2\right)^{-1/2} F\left[eS(\theta)\sin v + T(\theta)\frac{p}{r}\right] \tag{16}$$

$$\dot{e} = na^2\left(1-e^2\right)^{1/2} F\left[\begin{array}{c} S(\theta)\sin\theta + \\ T(\theta)\left[\cos(\theta)+\frac{1}{e}\left(1-\frac{r}{a}\right)\right] \end{array}\right] \quad (17)$$

$$\dot{i} = na^2\left(1-e^2\right)^{-1/2} FW\frac{r}{a}\cos u \quad (18)$$

$$\frac{\sin i\, d\Omega}{dt} = na^2\left(1-e^2\right)^{-1/2} FW\frac{r}{a}\sin u \quad (19)$$

$$\dot{\omega} = -\cos i\dot{\Omega} + \frac{na^2\left(1-e^2\right)^{1/2}}{e} + na^2\frac{\left(1-e^2\right)^{1/2}}{e}F \times\left[\begin{array}{c} -S(\theta)\cos\theta + \\ T(\theta)\left(1+\frac{r}{a}\right)\sin\theta \end{array}\right] \quad (20)$$

$$\dot{M} = n - 2na^2 FS(\theta)\frac{r}{a} - \left(1-e^2\right)^{1/2}\left(\dot{\omega}+\dot{\Omega}\cos i\right) \quad (21)$$

Mentioned parameters indicated $S(\theta), T(\theta)$ and $W(\theta)$, are force components of direct solar radiation in the radial direction, perpendicular to the radius and are perpendicular to the plane respectively.

$$\begin{Bmatrix} S(\theta) \\ T(\theta) \end{Bmatrix} = -\cos^2\frac{i}{2}\cos^2\frac{\varepsilon}{2}\begin{Bmatrix}\cos\\ \sin\end{Bmatrix}(\lambda_\otimes - u - \Omega) - \\ -\sin^2\frac{i}{2}\sin^2\frac{\varepsilon}{2}\begin{Bmatrix}\cos\\ \sin\end{Bmatrix}(\lambda_\otimes - u + \Omega) - \\ -\frac{1}{2}\sin i\sin\varepsilon\left[\begin{Bmatrix}\cos\\ \sin\end{Bmatrix}(\lambda_\otimes - u) - \begin{Bmatrix}\cos\\ \sin\end{Bmatrix}(-\lambda_\otimes - u)\right] - \\ -\sin^2\frac{i}{2}\cos^2\frac{\varepsilon}{2}\begin{Bmatrix}\cos\\ \sin\end{Bmatrix}(-\lambda_\otimes - u + \Omega) - \\ -\cos^2\frac{i}{2}\sin^2\frac{\varepsilon}{2}\begin{Bmatrix}\cos\\ \sin\end{Bmatrix}(-\lambda_\otimes - u - \Omega) \quad (22)$$

$$W = \sin i\cos^2\frac{\varepsilon}{2}\sin(\lambda_\otimes - \Omega) - \\ \sin i\sin^2\frac{\varepsilon}{2}\sin(\lambda_\otimes + \Omega) - \cos i\sin\varepsilon\sin\lambda_\otimes \quad (23)$$

which $\lambda_\otimes = \theta_\otimes + \omega_\otimes$, is the angle between the Sun position vector and the vernal equinox and also ε is the obliquity of the Sun to the equator which has the average value of 23.45^o.

For analyzing the shadow instantaneous effect, we refer to the pattern in [55]. This presentation suggests that assuming the Earth's shadow as cylindrical, the true anomaly angle (θ) corresponds to the angle of the satellite's entry and exit to the shadow, which satisfies this equation.

$$R_E^2(1+e\cos\theta)^2 + p^2(\beta_1\cos\theta + \beta_2\sin\theta)^2 - p^2 = 0 \quad (24)$$

in which R_E^2 is the radius of the Earth at the equator, (e) eccentricity of satellite orbit, $p = a(1-e^2)$, $\beta_1$and β_2 are

$$\beta_1 = \frac{\vec{R}_S.\,\vec{P}}{\left|\vec{R}_S\right|} \quad ; \quad \beta_2 = \frac{\vec{R}_S.\,\vec{Q}}{\left|\vec{R}_S\right|} \quad (25)$$

$\vec{R}_S$ is the Sun position vector in the inertial system and $\vec{P}$ and $\vec{Q}$ are

$$\vec{P} = \begin{bmatrix} \cos\omega\cos\Omega - \sin\omega\sin\Omega\cos i \\ \cos\omega\sin\Omega + \sin\omega\cos\Omega\cos i \\ \sin\omega\sin i \end{bmatrix} \quad (26)$$

$$\vec{Q} = \begin{bmatrix} -\sin\omega\cos\Omega - \cos\omega\sin\Omega\cos i \\ -\sin\omega\sin\Omega + \cos\omega\cos\Omega\cos i \\ \cos\omega\sin i \end{bmatrix} \quad (27)$$

The angle of shadow entry and exit can be calculated by arranging function (24) and solving the derived equation using recursive methods such as Newton-Raphson with constraints.

$$f(x) = Ax^2 + Bx + C\sqrt{1-x^2} + D = 0 \quad (28)$$

In the earlier equation $x = cos\theta$ and the condition for the answer is the following terms $f(1)f(-1) \le 0$, $-1 \le x \le 1$, then solving method such as Newton are used.

$$x_{n+1} = x_n - \frac{f(x)}{f'(x)} \quad ; \quad n = 0,1,2,3,... \quad (29)$$

To ensure the equation has been solved correctly, a momentary check is necessary.

$$|f(x)| \le Desired\ Tolerance \quad (30)$$

4. Earth Oblateness

As the influence of the Earth on the object is a conservative force and impact, we use the potential function gradient like $V(r) = -\mu/r$. The model described earlier would only be usable if the Earth was a complete spherical and was a homogeneous in mass distribution, whereas it is not like that, it needs to define the potential function for our planet. Supposing the Earth elliptical, we can generalize the potential function with a factor like $\beta(r,\varphi,\lambda)$ which is a function of position and geocentric latitude and longitude, as described in [57].

$$V(r) = -\frac{\mu}{r} + \beta(r,\phi,\lambda) \quad (31)$$

Calculating the coefficients of equations based on Earth gravity harmonics, solving Laplacian equations, and using spherical coordinates, we can determine the potential function, which can be expressed by the following series. The method of producing the potential

function and adjusting the coefficients is explained in [58].

$$V = -\frac{\mu}{r}\sum_{n=0}^{\infty}\left(\frac{r_e}{r}\right)^n \sum_{m=1}^{n} P_n^m(\cos\theta)\times \left[C_{nm}\cos m\phi + S_{nm}\sin m\phi\right] \tag{32}$$

By matching the spherical harmonics S_{nm} and C_{nm} to the Legendre polynomial series, the coefficients are classified into three categories representing the Earth, which P_n^m is the Legendre polynomial. Conservative forces can be expressed as a force component pattern. The force components derived from a non-spherical Earth model are analyzed using a spherical system to study the Gaussian Equation. Zonal harmonics are the only components included, as well as Legendre's polynomials and their extension described in [55] are used.

$$f_r = \frac{\mu}{r^2}\sum_{n=2}^{\infty} J_n(n+1)\left(\frac{R_e}{r}\right)^n P_n(\sin i\sin u) \tag{33}$$

$$f_t = -\frac{\mu}{r^2}\sin i\cos u\sum_{n=2}^{\infty} J_n\left(\frac{R_e}{r}\right)^n P_n'(\sin i\sin u) \tag{34}$$

$$f_n = -\frac{\mu}{r^2}\cos i\sum_{n=2}^{\infty} J_n\left(\frac{R_e}{r}\right)^n P_n'(\sin i\sin u) \tag{35}$$

In which P_n is Legendre polynomial and P_n' is the combination of the Legendre polynomial

c (36)

and $\alpha = \sin(i)\sin(u)$

5. The effect of third body

The third body produces an additional gravitational effect to that of the Earth.

$$V = \frac{\mu_3}{r_3}\left[\left(1+\frac{r^2}{r_3^2}-\frac{2r}{r_3}\cos\psi\right)^{-1/2} - \frac{r\cos\psi}{r_3}\right] \tag{37}$$

Potential function (38) in [59] is based on the viewpoint of Kozai - Kaufman in which subscript 3 belongs to perturbed object, μ_3 is the constant gravitational parameter and m_3 is the body mass of the third object (Sun or Moon). The distance of a satellite from the center of the Earth (r), and third object from the Earth center (r_3), along with the angle between their vectors (ψ), can be used to expand the potential function. By using the orbital elements of both objects, the potential function based on Kozai and Kaufman's viewpoint can be produced.

$$V = \frac{a^2 n_3^2}{2}\left(\frac{a_3}{r_3}\right)^3\left\{\begin{array}{c}\left[\frac{3}{2}\left(A^2+B^2\right)-1\right]\left(1+\frac{3e^2}{2}\right)\\ +\frac{3}{2}\left(A^2-B^2\right)\frac{5e^2}{2}\end{array}\right\} \tag{38}$$

and $\vec{A} = \vec{P}.\vec{e}_3$, $\vec{B} = \vec{Q}.\vec{e}_3$ and $\vec{P}, \vec{Q}$ are the unit vectors of perifocal coordinate system which had been mentioned in relation (27) and (28) and vector $\vec{e}_3$ is the unit vector directed to the third object.

$$\vec{e}_3 = \begin{bmatrix}\cos\Omega_3\cos u_3 - \sin\Omega_3\sin u_3\cos i_3\\ \sin\Omega_3\cos u_3 + \cos\Omega_3\sin u_3\cos i_3\\ \sin u_3\sin i_3\end{bmatrix} \tag{39}$$

u_3, i_3, Ω_3 are respectively the argument of latitude, inclination and RAAN of the third object. By expanding $A^2 + B^2$, $A^2 - B^2$ using the series and working on the potential function (39), the Lagrange equations can be derived to study the changes in orbital elements due to third body gravity.

$$\frac{da}{dt} = 0 \tag{40}$$

$$\frac{de}{dt} = -\frac{15}{8}e\gamma s(IMW) \tag{41}$$

$$\frac{di}{dt} = -\frac{3}{4}\frac{\gamma\csc i}{s}\left[\begin{array}{c}\left(1+\frac{3}{2}e^2\right)IPO+\\ \frac{5}{2}e^2(IMO-\cos i IMW)\end{array}\right] \tag{42}$$

$$\frac{d\Omega}{dt} = \frac{3}{4}\frac{\gamma}{s}\left[\begin{array}{c}\left(1+\frac{3}{2}e^2\right)\left(\frac{\cos i}{\sin i}IPS - IPC\right)\\ +\frac{5}{2}e^2\left(\frac{\cos i}{\sin i}IMS - IMC\right)\end{array}\right] \tag{43}$$

$$\frac{d\omega}{dt} = \frac{3}{2}s\gamma\left[\frac{3}{2}\left(A^2+B^2\right)-1+\frac{5}{2}\left(A^2-B^2\right)\right] - \cos i\frac{d\Omega}{dt} \tag{44}$$

$$\frac{dM}{dt} = n - 2\gamma\left\{\begin{array}{c}\left(1+\frac{3}{2}e^2\right)\left[\frac{3}{2}\left(A^2+B^2\right)-1\right]\\ +\frac{15}{4}e^2\left(A^2-B^2\right)\end{array}\right\} - \frac{3}{2}s^2\gamma\left[\frac{3}{2}\left(A^2+B^2\right)-1+\frac{5}{2}\left(A^2-B^2\right)\right] \tag{45}$$

so $S = \sqrt{1-e^2}$, $\gamma = \frac{n_3^2}{n}\left(\frac{a_3}{r_3}\right)^2 R_m$ and R_m is the mass ratio. So if the Moon is the third object $R_m = 1/27$, for the Sun $R_m = 1$ and parameters IMW, IMS, IMC, IMO, IPO, IPS and IPC are:

$$IMS = \begin{Bmatrix} -\sin i \sin^2 i_3 \cos 2\omega \\ +(1/4)\sin 2i_3 \begin{bmatrix} (1-\cos i)\cos(2\omega - \Delta\Omega) \\ -(1+\cos i)\cos(2\omega + \Delta\Omega) \end{bmatrix} \\ +(1/2)\sin i \sin i_3 [\cos 2(u_3 - \omega) + \cos 2(u_3 + \omega)] \\ +(1/4)\sin i_3 \begin{bmatrix} (1+\cos i)(1+\cos i_3)\cos(2u_3 - 2\omega - \Delta\Omega) \\ +(1-\cos i)(1-\cos i_3)\cos(2u_3 - 2\omega + \Delta\Omega) \\ -(1-\cos i)(1+\cos i_3)\cos(2u_3 + 2\omega - \Delta\Omega) \\ -(1+\cos i)(1-\cos i_3)\cos(2u_3 + 2\omega + \Delta\Omega) \end{bmatrix} \end{Bmatrix} \quad (46)$$

$$IPO = -(1/2)\sin i \begin{Bmatrix} \cos i \sin 2i_3 \sin \Delta\Omega + \sin i \sin^2 i_3 \sin 2\Delta\Omega \\ -(1/2)\sin i \begin{bmatrix} (1+\cos i_3)^2 \sin 2(u_3 - \Delta\Omega) \\ -(1-\cos i_3)^2 \sin 2(u_3 + \Delta\Omega) \end{bmatrix} \\ +\cos i \sin i_3 \begin{bmatrix} (1+\cos i_3)\sin(2u_3 - \Delta\Omega) \\ +(1-\cos i_3)\sin(2u_3 + \Delta\Omega) \end{bmatrix} \end{Bmatrix} \quad (47)$$

$$IPC = \begin{Bmatrix} \cos i\left[1 - (1/2)\sin^2 i_3\right] + (1/2)\sin i \sin 2i_3 \cos \Delta\Omega \\ -(1/2)\cos i \sin^2 i_3 \cos 2\Delta\Omega + (1/2)\cos i \sin^2 i_3 \cos 2u_3 \\ +(1/2)\sin i \sin i_3 \begin{bmatrix} (1-\cos i_3)\cos(2u_3 + \Delta\Omega) \\ -(1+\cos i_3)\cos(2u_3 - \Delta\Omega) \end{bmatrix} \\ -(1/4)\cos i \begin{bmatrix} (1+\cos i_3)^2 \cos 2(u_3 - \Delta\Omega) \\ +(1-\cos i_3)^2 \cos 2(u_3 + \Delta\Omega) \end{bmatrix} \end{Bmatrix} \quad (48)$$

$$IPS = \begin{Bmatrix} \sin i \sin^2 i_3 + (1/2)\cos i \sin 2i_3 \cos \Delta\Omega - \sin i \sin^2 i_3 \cos 2u_3 \\ +(1/2)\cos i \sin i_3 \begin{bmatrix} (1-\cos i_3)\cos(2u_3 + \Delta\Omega) \\ -(1+\cos i_3)\cos(2u_3 - \Delta\Omega) \end{bmatrix} \end{Bmatrix} \quad (49)$$

$$IMW = \begin{Bmatrix} (1/2)\sin^2 i(3\sin^2 i_3 - 2)\sin 2\omega \\ -(1/4)\sin^2 i_3 \left[(1-\cos i)^2 \sin 2(\omega - \Delta\Omega) + (1+\cos i)^2 \sin 2(\omega + \Delta\Omega)\right] \\ +(1/2)\sin i \sin 2i_3 \left[(1+\cos i)^2 \sin(2\omega + \Delta\Omega) - (1-\cos i)^2 \sin(2\omega - \Delta\Omega)\right] \\ +(1/8) \begin{bmatrix} (1+\cos i)^2(1+\cos i_3)^2 \sin 2(u_3 - \omega - \Delta\Omega) \\ +(1-\cos i)^2(1-\cos i_3)^2 \sin 2(u_3 - \omega + \Delta\Omega) \\ -(1-\cos i)^2(1+\cos i_3)^2 \sin 2(u_3 + \omega - \Delta\Omega) \\ -(1+\cos i)^2(1-\cos i_3)^2 \sin 2(u_3 + \omega + \Delta\Omega) \end{bmatrix} \\ +(3/4)\sin^2 i \sin^2 i_3 [\sin 2(u_3 - \omega) - \sin 2(u_3 + \omega)] \\ +(1/2)\sin i \sin i_3 \begin{bmatrix} (1+\cos i)(1+\cos i_3)\sin(2u_3 - 2\omega - \Delta\Omega) \\ +(1-\cos i)(1-\cos i_3)\sin(2u_3 - 2\omega + \Delta\Omega) \\ +(1-\cos i)(1+\cos i_3)\sin(2u_3 + 2\omega - \Delta\Omega) \\ +(1+\cos i)(1-\cos i_3)\sin(2u_3 + 2\omega + \Delta\Omega) \end{bmatrix} \end{Bmatrix} \quad (50)$$

$$IMC = \begin{Bmatrix} -(1/4)\sin i \sin 2i_3 [\cos(2\omega - \Delta\Omega) + \cos(2\omega + \Delta\Omega)] \\ +\cos i\left[(1/2)\sin^2 i_3 - 1\cos 2\omega\right] \\ +(1/4)\sin^2 i_3 [(1+\cos i)\cos 2(\omega + \Delta\Omega) - (1-\cos i)\cos 2(\omega - \Delta\Omega)] \\ +(1/8)\sin^2 i_3 \begin{bmatrix} (1+\cos i)(1+\cos i_3)^2 \cos 2(u_3 - \omega - \Delta\Omega) \\ +(1-\cos i)(1-\cos i_3)^2 \cos 2(u_3 - \omega + \Delta\Omega) \\ -(1-\cos i)(1+\cos i_3)^2 \cos 2(u_3 + \omega - \Delta\Omega) \\ +(1+\cos i)(1-\cos i_3)^2 \cos 2(u_3 + \omega + \Delta\Omega) \end{bmatrix} \\ +(1/4)\sin i \sin i_3 (1+\cos i_3)[\cos(2u_3 - 2\omega - \Delta\Omega) + \cos(2u_3 + 2\omega - \Delta\Omega)] \\ -(1/4)\sin i \sin i_3 (1-\cos i_3)[\cos(2u_3 - 2\omega + \Delta\Omega) + \cos(2u_3 + 2\omega + \Delta\Omega)] \\ -(1/4)\cos i \sin^2 i_3 [\cos 2(u_3 - \omega) + \cos 2(u_3 + \omega)] \end{Bmatrix} \quad (51)$$

$$IMO = (1/4)\times \begin{Bmatrix} \sin^2 i_3 \begin{bmatrix} (1-\cos i)^2 \sin 2(\omega - \Delta\Omega) \\ -(1+\cos i)^2 \sin 2(\omega + \Delta\Omega) \end{bmatrix} \\ +\sin i \sin 2i_3 [(1+\cos i)\sin(2\omega + \Delta\Omega) + (1-\cos i)\sin(2\omega - \Delta\Omega)] \\ +(1/2) \begin{bmatrix} (1+\cos i^2)(1+\cos i_3)^2 \sin 2(u_3 - \omega - \Delta\Omega) \\ -(1-\cos i^2)(1-\cos i_3)^2 \sin 2(u_3 - \omega + \Delta\Omega) \\ +(1-\cos i^2)(1+\cos i_3)^2 \sin 2(u_3 + \omega - \Delta\Omega) \\ -(1+\cos i^2)(1-\cos i_3)^2 \sin 2(u_3 + \omega + \Delta\Omega) \end{bmatrix} \\ +\sin i \sin i_3 \begin{bmatrix} (1+\cos i)(1+\cos i_3)\sin(2u_3 - 2\omega + \Delta\Omega) \\ -(1-\cos i)(1-\cos i_3)\sin(2u_3 - 2\omega + \Delta\Omega) \\ -(1-\cos i)(1+\cos i_3)\sin(2u_3 + 2\omega - \Delta\Omega) \\ +(1+\cos i)(1-\cos i_3)\sin(2u_3 + 2\omega + \Delta\Omega) \end{bmatrix} \end{Bmatrix} \quad (52)$$

$$IMW = \frac{\partial\left(A^2 - B^2\right)}{\partial\omega};\ IPO = \frac{\partial\left(A^2 + B^2\right)}{\partial\Omega} \quad (53)$$

$$IPS = \frac{\partial\left(A^2 + B^2\right)}{\partial \sin i}; IPC = \frac{\partial\left(A^2 + B^2\right)}{\partial \cos i}$$

$$IMS = \frac{\partial\left(A^2 - B^2\right)}{\partial \sin i};\ IMC = \frac{\partial\left(A^2 - B^2\right)}{\partial \cos i}$$

$$IMO = \frac{\partial\left(A^2 - B^2\right)}{\partial\Omega}$$

6. Earth Solid Tides

The Sun and Moon's gravitational forces cause the Earth to experience solid tides, resulting in changes in its shape similar to an elastic body. The potential function and the harmonics of Earth's gravity will undergo changes from the normal mode.

Table 1- Gravitational forces applied to the Moon and Earth by gravitation body

Moon Gravitational force due to the Earth	1.82×1018 N
Earth Gravitational force due to the Moon	6.69×1018 N
Earth Gravitational force due to the Sun	3.02×1018 N

Earth experiences 3.5 times more gravitational force from the Moon than the Moon experiences from the Earth, and 2 times more than the Sun's gravitational force. The impact of the Moon's gravity on Earth is vital compared to the Sun's. A potential function presents changes over times that depend on spherical gravity

harmonics. Most articles and patterns give more importance to the gravitational effect of the Moon, whereas [38] and this article present both the effects of the Sun and Moon's gravity simultaneously.

$$V = k_2 \frac{R^5}{a^3}\left(1-e^2\right)^{-3/2} \times \left\{ m_m n_m^2 \left(\frac{a_m}{r_m^*}\right)^3 W_m + m_S n_S^2 \left(\frac{a_S}{r_S^*}\right)^3 W_S \right\} \tag{54}$$

that indicators W_S and W_m will be the Moon and Sun effects and in equation (56), f_m^* and ω_m are respectively the true anomaly and argument of perigee of the Moon

$$\begin{aligned} W_m = {} & \frac{1}{4}\left(1-\frac{3}{2}\sin^2 i\right)\left(1-\frac{3}{2}\sin^2 i_m\right) \\ & + \frac{3}{16}\sin 2i \sin 2i_m \cos\theta_m + \frac{3}{16}\sin^2 i \sin^2 i_m \cos 2\theta \\ & + \frac{3}{8}\sin^2 i_m\left(1-\frac{3}{2}\sin^2 i\right)\cos 2\left(f_m^* + \omega_m\right) \\ & + \frac{3}{8}\sin^2 i \cos^4 \frac{i_m}{2}\cos 2\left(f_m^* + \omega_m - \theta_m\right) \\ & - \frac{3}{8}\sin 2i \sin i_m \cos^2 \frac{i_m}{2}\cos\left(2f_m^* + 2\omega_m - \theta_m\right) \\ & + \frac{3}{8}\sin^2 i \cos^4 \frac{i_m}{2}\cos 2\left(f_m^* + \omega_m + \theta_m\right) \\ & + \frac{3}{8}\sin 2i \sin i_m \sin^2 \frac{i_m}{2}\cos\left(2f_m^* + 2\omega_m + \theta_m\right) \end{aligned} \tag{55}$$

If the alteration in the shape of the Earth occurs entirely along the line connecting the Moon and Earth or the line connecting the Sun and the Earth, and there is no variation in the phase, then we can apply the parameters in equation (56) in this manner:

$$\begin{cases} a_m / r_m^* = a_S / r_S^* \\ f_m^* + \omega_m = \lambda_m \\ f_S^* + \omega_S = \lambda_S \\ \theta = \theta_m = \theta_S = \Omega \end{cases} \tag{56}$$

By utilizing the potential function and the Lagrange equations, we can study and model the variations in perturbed orbital elements as opposed to changes in the Earth's shape due to gravitational forces from the Sun and Moon. Different sources such as [60] have presented the pattern of solid tides on Earth and their effects on the perturbed acceleration in the inertial system. [60] have explained how the potential function is affected by changes in the Earth's shape and how this affects the spherical gravity harmonics coefficient.

Disturbed acceleration in an inertia system for analyzing the Cowell method, expressed, and it leads to equation (57),

$$\ddot{\vec{r}}_{Tide} = \frac{3}{2}\frac{\mu}{\left|\vec{r}_{s,m}\right|^3}\frac{R_e^5}{\left|\vec{r}\right|^4}\left[\begin{array}{l} \left(1-5\cos^2\theta\right)\dfrac{\vec{r}}{\left|\vec{r}\right|} + \\ 5\cos\theta\dfrac{\vec{r}_{s,m}}{\left|\vec{r}_{s,m}\right|} \end{array}\right] \tag{57}$$

In which index S and m indicate the effects of the Sun and the Moon and this pattern only consist of J_2 major effects and θ is the angle between the satellite position vector $\vec{r}$ and the Sun or Moon position vector $\vec{r}_{s,m}$ in inertial system and R_e is the radius of the Earth in equator.

7. General relativity effects

The general theory of relativity proposed by Einstein revealed that Newton's law of gravitation is not precise and requires revision in extremely strong gravitational fields. According to Newton, light always moves in a straight line, but Einstein proved that when light passes near an object with a significant gravitational field, its direction is shifted.

In the Earth's reference frame, the primary relativistic effects affecting satellite trajectories can be categorized into three main components. The first is the Schwarzschild effect, caused by Earth's static gravitational field. The second is the Lense-Thirring effect (or frame-dragging), arising from Earth's rotation distorting spacetime and the third is the de Sitter effect (geodetic precession), resulting from Earth's orbital motion around the Sun.

$$\begin{aligned} \ddot{\vec{r}}_{Rel} = {} & -\frac{\mu}{c^2\left|\vec{r}\right|^3}\left[\left(4\frac{\mu}{\left|\vec{r}\right|} - \gamma\left|\dot{\vec{r}}\right|^2\right)\vec{r} + 4\left(\vec{r}.\dot{\vec{r}}\right)\dot{\vec{r}}\right] + \\ & \frac{2\mu}{c^2\left|\vec{r}\right|^3}\left[\frac{3}{\left|\vec{r}\right|^2}\left(\vec{r}\times\dot{\vec{r}}\right)\left(\vec{r}\times\vec{J}\right) + \left(\dot{\vec{r}}\times\vec{J}\right)\right] + \\ & 3\left[\dot{\vec{R}}_s \times \left(\frac{\mu_s \times \vec{R}_s}{c^2\left|\vec{R}_s\right|^3}\right)\right]\times\dot{\vec{r}} \end{aligned} \tag{58}$$

The first line describes the so-called Schwarzschild term , the second is the frame-dragging gravitomagnetic Lense–Thirring effect, whereas the third corresponds to the de Sitter effect.

Many analyses, particularly those examining the contributions of these effects in GNSS satellites, indicate that the first effect (Schwarzschild) is significantly more substantial than the subsequent two. On Galileo satellites E14, the Schwarzschild accelerations on Galileo E14 range between 123.3×10^{-12} and 388.3×10^{-12} m·s^{-2}, see Fig. 1. The de Sitter accelerations are between -5.6×10^{-12} and -25.3×10^{-12} m·s^{-2}, whereas Lense–Thirring are between 0.7×10^{-12} and 4.6×10^{-12} m·s^{-2}. Hence, for Galileo satellites, the Schwarzschild accelerations introduce stronger perturbations than de Sitter and the Lense–Thirring

effect by two and one order of magnitude, respectively. Therefore, in this study, we focus on the first effect, and the derivation of the equations is based on this consideration [47].

The summary of general relativity is that mass tells space-time how to curve. Using of general relativity theory equations allows modeling of this question, which is unanalyzable by Newton's laws. In [45] , a perturbed potential function resulting from general relativity effects is explained. [61] Study contains the development of a perturbed force component based on Gauss equations.

$$R = \frac{c^2 m^2}{r^2}\left(\frac{2}{r} + \frac{1 - e^2 + 4e^2 \sin^2\theta}{p}\right) + \frac{4}{5} c p^{1/2} m^{3/2} \omega_0 R_e^2 \cos i \frac{1}{r^4} - \frac{2m\omega_0^2 R_e^2}{5r^2} + \frac{3m\omega_0^2 R_e^4}{35 r^4}\left[3\sin^2(\omega+\theta)\sin^2 i - 1\right] \quad (59)$$

$$S = \frac{4c^2 m^2}{r^3} e \sin\theta - \frac{4}{5} c p^{-1/2} m^{3/2} \omega_0 R_e^2 e \cos i \sin\theta \frac{1}{r^3} - \frac{6}{35} m\omega_0^2 R_e^4 \sin^2 i \sin(\omega+\theta)\cos(\omega+\theta)\frac{1}{r^4} \quad (60)$$

$$W = \frac{4}{5} c p^{-1/2} m^{3/2} \omega_0 R_e^2 \sin i \frac{1}{r^3} \times \begin{bmatrix} -e\sin\omega + \\ (2 + 3e\cos\theta)\sin(\omega+\theta) \end{bmatrix} - \frac{6}{35} m\omega_0^2 R_e^4 \sin i \cos i \sin(\omega+\theta)\frac{1}{r^4} \quad (61)$$

Thus, assume c the speed of light, R_e the Earth radius and ω_0 angular speed of Earth rotation

$$\frac{d\Omega}{d\theta} = \frac{\sin(\omega+\theta)}{c^2 mp \sin i} r^3 W \quad (62)$$

$$\frac{di}{d\theta} = \frac{\cos(\omega+\theta)}{c^2 mp} r^3 W \quad (63)$$

$$\frac{d\omega}{d\theta} = -\frac{\cos\theta}{c^2 me} r^2 R + \frac{(2 + e\cos\theta)\sin\theta}{c^2 mpe} r^3 S - \frac{\sin(\omega+\theta)\cot i}{c^2 mp} r^3 W \quad (64)$$

$$\frac{dM}{d\theta} = -\frac{\left(1-e^2\right)^{1/2}}{c^2 mpe}\left(2e - \cos\theta - e\cos^2\theta\right) r^3 R - \frac{\left(1-e^2\right)^{1/2}}{c^2 mpe}(2 + e\cos\theta)\sin\theta\, r^3 S \quad (65)$$

$$\frac{dt}{d\theta} = \frac{r^2}{cm^{1/2} p^{1/2}} \quad ; \quad n = cm^{1/2} p^{-3/2}\left(1 - e^2\right)^{3/2} \quad (66)$$

Cowell method in orbital elements variation can be used to study the effect of relativistic effects based on perturbed acceleration in inertial frame [47] and [59].

8. Albedo

Satellites are subject to indirect solar radiation effects, as well as direct effects called Albedo. The satellite is affected by this effect caused by the reflection of direct solar radiation from the Earth and is greatly influenced by factors such as clouds and atmosphere. According to most references, including [55], these radiations are found along the radiant and consist of approximately 30% direct solar radiation. Assuming the above, we can analyze the effect of the albedo pattern using Gauss equations.

$$f_r|_{albedo} = 0.3;\ f_t = 0;\ f_n = 0 \quad (67)$$

9. Fundamental Theory of Orbit Perturbations

Generally, the equations and analysis methods for disturbed orbital effects are divided into three categories: Lagrange equations, equations of Gauss, and Cowell method. Lagrange equations use disturbed potential function V specific to conservative forces, making analysis of non-conservative forces impossible. The satellite is subject to a constant gravitational parameter $-\mu/r^3$ at all times. The perturbed force on the satellite is believed to be a gradient of a potential function. The partial derivatives of the disturbed potential function are assumed to be equal to the perturbed acceleration.

$$\ddot{\vec{r}} = -\mu\frac{\vec{r}_i}{r^3} + \nabla F \quad ; V = -F \quad (68)$$

Thus, according to [55] and [58], Lagrange disturbed differential equations are:

$$\dot{a} = -\frac{2}{na}\frac{\partial F}{\partial M} \quad (69)$$

$$\dot{e} = \frac{1-e^2}{na^2 e}\left(\frac{\partial F}{\partial M} - \left(1-e^2\right)^{-1/2}\frac{\partial F}{\partial \omega}\right) \quad (70)$$

$$\dot{i} = \frac{1}{na^2\sqrt{\left(1-e^2\right)}}\left(\cot i\,\frac{\partial F}{\partial \omega} - \csc i\,\frac{\partial F}{\partial \Omega}\right) \quad (71)$$

$$\dot{\omega} = -\frac{\left(1-e^2\right)^{1/2}}{na^2e}\frac{\partial F}{\partial e} - \frac{\cot i}{na^2\left(1-e^2\right)^{1/2}}\frac{\partial F}{\partial i} \tag{72}$$

$$\dot{\Omega} = -\frac{\csc i}{na^2\left(1-e^2\right)^{1/2}}\frac{\partial F}{\partial i} \tag{73}$$

$$\dot{M} = n - \frac{2}{na}\frac{\partial F}{\partial a} - \frac{1-e^2}{na^2e}\frac{\partial F}{\partial e} \tag{74}$$

$$\ddot{\vec{r}} = -\mu\frac{\vec{r}_i}{r^3} + \nabla F \quad ; V = -F \tag{75}$$

Gauss equation states that the perturbed forces can be both conservative and non-conservative. If the components of the disturbed forces are available on 3 along the radial $\vec{f}_r$, tangential $\vec{f}_t$ and $\vec{f}_n$ perpendicular to the orbit, you can analyze the orbital elements by Gauss equations and the process of equation production is mentioned in [51] and [52] by details.

$$\dot{a} = -\frac{2a^2}{\sqrt{\mu P}}\left\{f_r e\sin\theta + f_t\left(1+e\cos\theta\right)\right\} \tag{76}$$

$$\dot{e} = \sqrt{\frac{P}{\mu}}\left[f_r\sin\theta + f_t\left(\cos\theta+\cos E\right)\right] \tag{77}$$

$$\dot{\Omega}\sin i = \left(\mu P\right)^{-1/2} r\, f_n \sin u \tag{78}$$

$$\dot{i} = \left(\mu P\right)^{-1/2} r\, f_n \cos u \tag{79}$$

$$\dot{\omega} + \dot{\Omega}\cos i = \frac{1}{e}\left(\frac{P}{\mu}\right)^{1/2}\left\{-f_r\cos\theta + f_t\left(1+\frac{r}{P}\right)\sin\theta\right\} \tag{80}$$

$$\dot{M} = n + \frac{1-e^2}{nae}\begin{Bmatrix}\left[\frac{-2e}{1+e\cos(\theta)}+\cos(\theta)\right]f_r \\ -\left[1+\frac{1}{1+e\cos(\theta)}\right]\sin(\theta) f_t\end{Bmatrix} \tag{81}$$

We can investigate the change of orbital elements by solving the main equation including disturbed acceleration in inertial system with the Cowell method (70). However, the initial conditions to solve the main equation in the inertial frame are the vectors $\vec{r}_0$ and $\dot{\vec{r}}_0$. So at the beginning we have to transform the initial conditions of orbital elements $(a_0, e_0, i_0, \omega_0, \Omega_0, \theta_0)$ to position vector of $\vec{r}_0$,and initial speed $\dot{\vec{r}}_0$ in inertial system, then solving equation (69) and by instant producing $\vec{r}$ and $\dot{\vec{r}}$ in inertial system, we can transform vectors $\vec{r}$ and $\dot{\vec{r}}$ with another process to orbital elements $(a, e, i, \omega, \Omega, \theta)$ which is stated by details in [62] and [63].

10. Simulation

Three orbit types have been studied and simulated to investigate all discussed perturbation influences in this paper. "Table 2" characteristic and a collective feature based on an artificial satellite can be found in the three type orbit studied.

Table 2- Characteristics of the orbits

Properties	Orbit A	Orbit B	Orbit C
	LEO (km)	MEO(km)	GPS(km)
i=55°	h_p=245	r_p=11940	r_p=20138
$\omega = \Omega = 0$	h_a=378	r_a=12060	r_a=20225
$m = 27\,Kg$	a=6689.63	a=12000	a=20182
Dim: 40Cm^3	e=0.00994	e=0.005	e=0.00218

The initial parameters for solving the perturbed equation are identical to the initial conditions of the orbits. The selected time is chosen for the actual detumbling process time of a sample LEO satellite, which lasts about 4 orbits, and has no other reason. Changes in all the graphs of a are measured in meters, while changes in (i, Ω, ω, M) are measured in degrees. All charts show the deviation of orbital elements from their initial value $(\alpha - \alpha_0)$. Simulations have been executed in Simulink environment. The choice between explicit and implicit methods depends on the stiffness of the problem, computational efficiency, and accuracy requirements. For most orbital mechanics problems (e.g., satellite propagation, interplanetary trajectories, use ODE45 (RK4) or ODE113 (Adams). For stiff problems (e.g., low-perigee orbits, high eccentricity, drag-dominated cases), use ode15s (BDF) or ODE23t (Trapezoidal). For high-precision long-term simulations (e.g., space debris, lunar missions). In Summary Explicit methods (ODE45, ODE113) are preferred for most orbital ODE) are needed for stiff cases (e.g., atmospheric drag, high-fidelity perturbations) and Hybrid approaches (e.g., variable-step solvers) often work best in practice. Since this study did not impose specific constraints on computational time, and to prevent unwanted errors in long-term effects including shadow effects and third-body perturbations, it was decided to use variable time step for all calculations. The solver was selected automatically. Numerical simulations demonstrate robust stability with adaptive time-stepping, but enforcing a minimum time step ($\Delta t \geq 1000$ s) in long-term analyses leads to divergence in some cases. This highlights the importance of temporal resolution in maintaining numerical stability, as constrained step sizes can fail to capture critical dynamics, resulting in solution instability over extended durations.

11. Results

Through the utilization of the patterns to examine the effect of perturbations and the simulation output, as indicated in "Figure 1", one can detect the impact of drag in the LEO orbit, which leads to a decrease in energy and orbit altitude. It is clear that secular changes occur in the semi-major (a) axis and eccentricity (e). Additionally, the sensitivity analysis to variations in the drag coefficient and solar activities sweeping is presented in "Figure 2" and "Figure 3".

Taking into consideration the regional and meridional winds, it can also be noted that small changes occur on inclination (i) and longitude of ascending node (Ω) that these changes will be of great importance in the long term. Nonetheless, the reduction of orbit altitude may result in a shorter orbit lifetime, particularly for satellites with low eccentricity that have a lifespan ending at an altitude of 120 km. Table 3 demonstrates that if the amount of drag coefficient (C_d) increases, the lifetime of satellite decreases and by increasing the value of solar flux index ($F_{10.7}$), the lifetime of the satellite would decrease too. For better understanding, due to the dependence of perturbations on orbital height, the variations in orbital elements caused by drag are presented for Orbit A, along with other relevant diagrams for Orbit B.

Table 3- Initial estimates of orbit lifetime (days)
(M=16kg ; S=0.16m^2)

	$F_{10.7}$=250	$F_{10.7}$=180	$F_{10.7}$=120	$F_{10.7}$=80
Cd=2	17	25	39	60
Cd=2.2	16	23	35	55
Cd=2.4	14	21	33	50
Cd=2.6	13	19	29	46

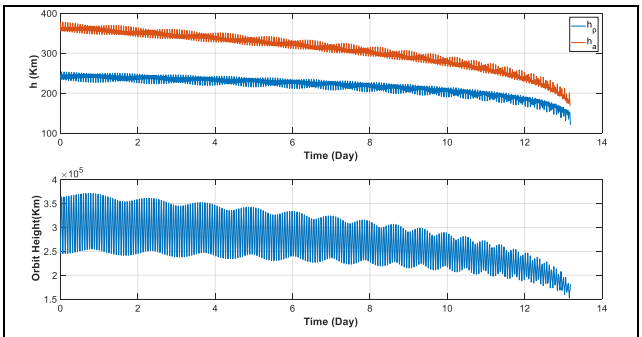

Figure 1- Sample variation of orbit height, h_p and h_a during lifetime (C_d=2.6, F1$_{0.7}$=250)

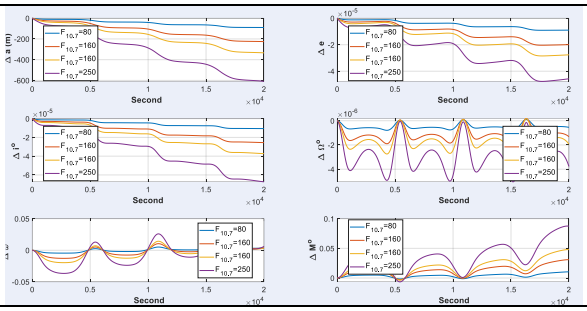

Figure 2- Variations in OE of Orbit B were evaluated through systematic sweeps of ($F_{10.7}$)

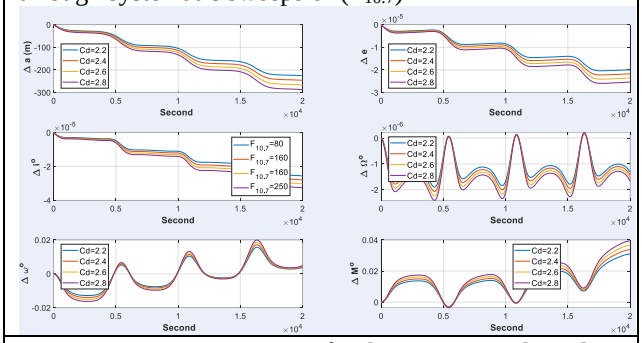

Figure 3- Variations in OE of Orbit B were evaluated through systematic sweeps of (C_d)

The impact of direct solar radiation for LEO orbit is shown in "Figure 4" that these changes for reflection coefficient value of ($C_p = 1$).

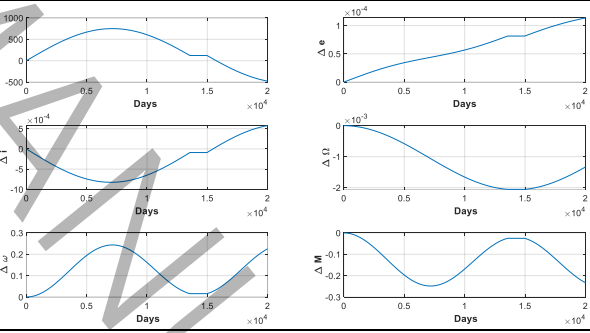

Figure 4-Variation of OE caused by direct solar radiation in orbit B

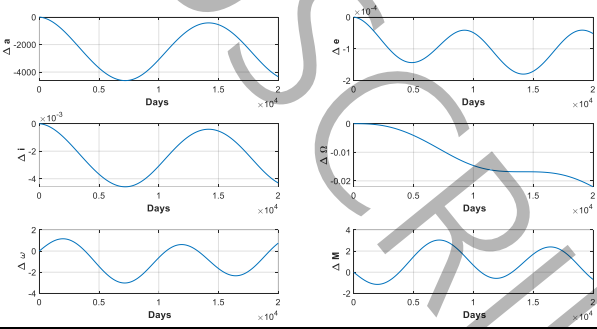

Figure 5- Variation of OE caused by Earth oblateness up to J_{10} in orbit B

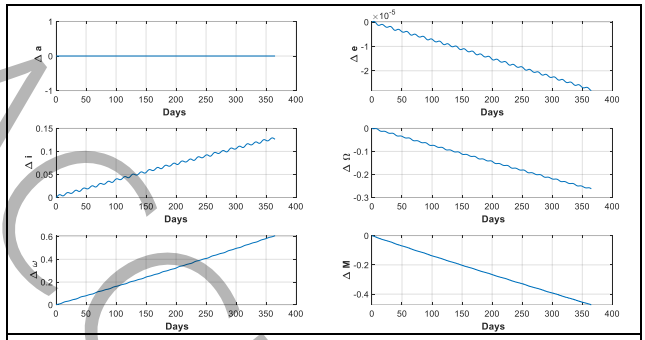

Figure 6- Variation of OE caused by Moon gravity in orbit B

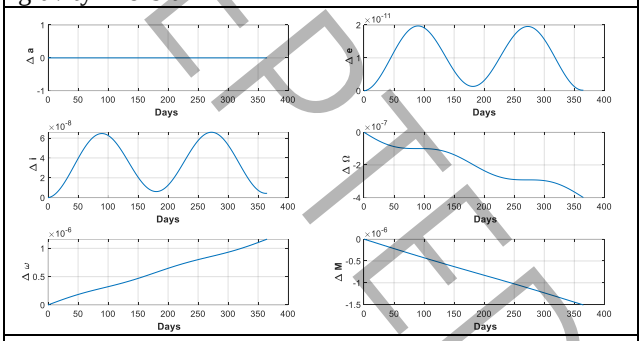

Figure 7- Variation of OE caused by Sun gravity in orbit B

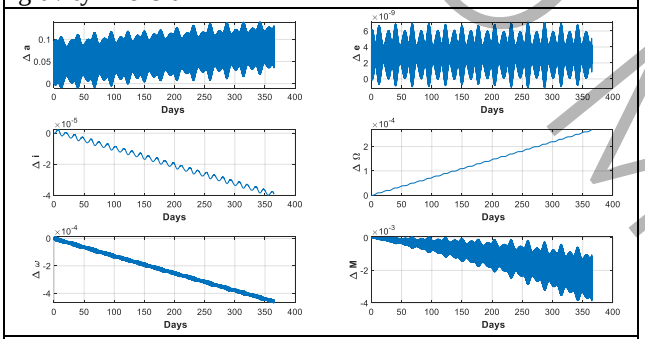

Figure 8- Variation of OE caused by solid tides due to Moon in orbit B

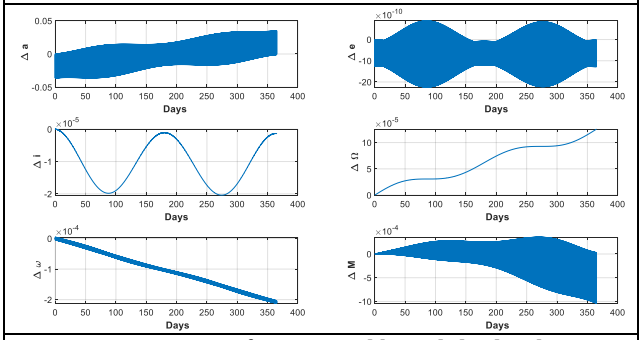

Figure 9- Variation of OE caused by solid tides due to Sun in orbit B

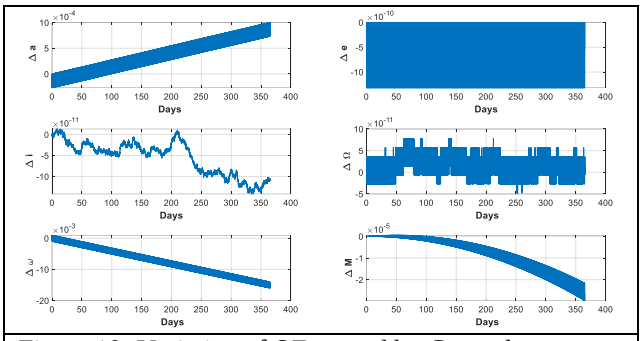

Figure 10- Variation of OE caused by General Relativity in orbit B

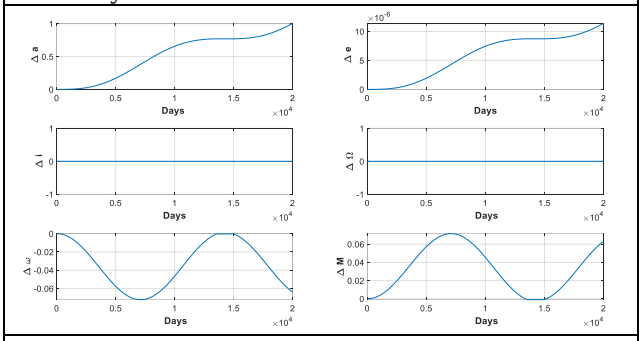

Figure 11- Variation of OE caused by solar radiation reflected in orbit A

Consequently, "Figure 5" displays how the Earth's oblateness can cause fundamental variations for the secularity of changes (ω, Ω, M) and high periodic changes on (a).

The outcome of the third body, such as the Moon in "Figure 6" and the Sun in "Figure 7", shows that while these adjustments are slight and the impact of the Moon is much greater, the long-term tendency of changes in the time span is of paramount importance.

The solar and lunar gravitational force, relative to their positions on the Earth, can impact the Earth's shape and orbital elements. Depending on the position of the Sun and Moon relative to Earth, their gravity can impact the planet's shape. Earth solid tides on orbital elements depicts in the "Figure 8" and "Figure 9".

"Figure 10" displays the effects of general relativity, which have minor changes. However, the impact of solar radiation reflected from the Earth (Albedo) also brings about long-term shifts in semi-major axis and periodic alterations in eccentricity and other orbital elements. This impact, as stated in "Figure 11", is much smaller than the impact of solar radiation pressure.

"Table 4" to "Table 9" illustrates the most significant fluctuations in orbital elements for three orbit types, rather than all disruptions.

Table 4- Maximum changes of orbital elements in orbit A

Perturbations	Δi°	Δe	Δa (m)
Earth Oblateness[1]	4.6×10^{-2}	1.7×10^{-3}	15427.2
Atmosphere Drag[1]	2.32×10^{-5}	1.85×10^{-5}	205.12
Direct solar radiation[2]	3.27×10^{-4}	5.67×10^{-5}	101.432
Moon Gravity[2]	4.13×10^{-5}	2.15×10^{-8}	0
Sun Gravity[2]	0	0	0
solid tides due to the Moon[3]	2.07×10^{-6}	5.54×10^{-8}	0.288
solid tides due to the Sun[3]	5.2×10^{-7}	1.51×10^{-8}	0.113
solid tides due to the Sun & Moon[3]	2.34×10^{-6}	4.4×10^{-8}	0.179
General relativity[3]	3.34×10^{-13}	4.04×10^{-9}	4.7×10^{-3}
Albedo[1]	0	6.77×10^{-6}	0.902

Superscripts: 1.Gauss method, 2. Lagrange method, 3.Cowell method

Table 5- Maximum change of orbital elements in orbit A

Perturbations	**ΔM**	**$\omega\Delta$**	**$\Omega\Delta$**
Earth Oblateness[1]	33.28	30.31	1.1
Atmosphere Drag[1]	3.07×10^{-2}	2.52×10^{-2}	1.88×10^{-6}
Direct solar radiation[2]	2×10^{-2}	7.8×10^{-3}	2.21×10^{-4}
Moon Gravity[2]	5.65×10^{-5}	7.6×10^{-5}	4.81×10^{-5}
Sun Gravity[2]	5.51×10^{-10}	1.8×10^{-10}	9.93×10^{-11}
solid tides due to the Moon[3]	7.57×10^{-5}	1.84×10^{-4}	2.37×10^{-7}
solid tides due to the Sun[3]	2.85×10^{-10}	9.28×10^{-5}	7.82×10^{-6}
solid tides due to the Sun & Moon[3]	4.7×10^{-5}	1.54×10^{-4}	7.6×10^{-6}
General relativity[3]	1.2×10^{-6}	2.47×10^{-5}	1.09×10^{-12}
Albedo[1]	1.83×10^{-3}	1.9×10^{-3}	0

Superscripts: 1.Gauss method, 2. Lagrange method, 3.Cowell method

Table 6- Maximum change in orbital elements in orbit B

Perturbations	Δi°	Δe	Δa (m)
Earth Oblateness[1]	1.32×10^{-2}	5.1×10^{-4}	7932.5
Atmosphere Drag[1]	0	0	0
Direct solar radiation[2]	5.91×10^{-4}	8.24×10^{-5}	314.66
Moon Gravity[2]	9.93×10^{-5}	2.6×10^{-8}	0
Sun Gravity[2]	0	0	0
solid tides due to the Moon[3]	2.68×10^{-7}	1.72×10^{-8}	0.1576
solid tides due to the Sun[3]	1.16×10^{-7}	3.56×10^{-9}	6.07×10^{-2}
solid tides due to the Sun & Moon[3]	3.32×10^{-7}	1.37×10^{-8}	9.72×10^{-2}
General relativity[3]	3.98×10^{-13}	2.21×10^{-9}	7.09×10^{-4}
Albedo[1]	0	9.23×10^{-6}	1.1088

Superscripts: 1.Gauss method, 2. Lagrange method, 3.Cowell method

Table 7- Maximum changes of orbital elements in orbit B

Perturbations	ΔM	$\omega\Delta$	$\Omega\Delta$
Earth Oblateness[1]	7.94	7.67	0.143
Atmosphere Drag[1]	0	0	0
Direct solar radiation[2]	4.63×10^{-2}	4.19×10^{-2}	7.22×10^{-4}
Moon Gravity[2]	1.39×10^{-4}	1.77×10^{-4}	1.15×10^{-4}
Sun Gravity[2]	4.25×10^{-10}	4.34×10^{-10}	2.42×10^{-10}
solid tides due to the Moon[3]	8.94×10^{-6}	1.09×10^{-4}	4.97×10^{-8}
solid tides due to the Sun[3]	3.41×10^{-6}	5.51×10^{-5}	1.01×10^{-6}
solid tides due to the Sun & Moon[3]	5.53×10^{-6}	8.89×10^{-5}	9.91×10^{-7}
General relativity[3]	3.23×10^{-8}	2.55×10^{-5}	1.09×10^{-12}
Albedo[1]	1.13×10^{-2}	1.14×10^{-2}	0

Superscripts: 1.Gauss method, 2. Lagrange method, 3.Cowell method

Table 8- Maximum changes of orbital elements in orbit C

Perturbations	Δi°	Δe	Δa (m)
Earth Oblateness[1]	4.6×10^{-3}	1.79×10^{-4}	4625.1
Atmosphere Drag[1]	0	0	0
Direct solar radiation[2]	1.4×10^{-3}	1.13×10^{-4}	1227.1
Moon Gravity[2]	2.16×10^{-4}	2.47×10^{-8}	0
Sun Gravity[2]	0	1.28×10^{-15}	0
solid tides due to the Moon[3]	4.57×10^{-8}	6.09×10^{-9}	9.3×10^{-2}
solid tides due to the Sun[3]	3.31×10^{-8}	1.26×10^{-9}	3.6×10^{-2}
solid tides due to the Sun & Moon[3]	5.06×10^{-8}	4.82×10^{-9}	5.7×10^{-2}
General relativity[3]	4.4×10^{-13}	1.31×10^{-9}	2.56×10^{-4}
Albedo[1]	0	1.14×10^{-5}	1

Superscripts: 1.Gauss method, 2. Lagrange method, 3.Cowell method

Table 9- Maximum changes of orbital elements in orbit C

Perturbations	**ΔM**	**$\omega\Delta$**	**$\Omega\Delta$**
Earth Oblateness[1]	4.19	4.17	2.19×10^{-2}
Atmosphere Drag[1]	0	0	0
Direct solar radiation[2]	0.246	0.243	2.1×10^{-3}
Moon Gravity[2]	3.34×10^{-4}	4.58×10^{-4}	2.52×10^{-4}
Sun Gravity[2]	1.09×10^{-9}	10^{-9}	5.39×10^{-10}
solid tides due to the Moon[3]	1.51×10^{-6}	8.79×10^{-5}	1.41×10^{-8}
solid tides due to the Sun[3]	5.97×10^{-7}	3.78×10^{-5}	1.55×10^{-7}
solid tides due to the Sun & Moon[3]	9.17×10^{-7}	7.1×10^{-5}	1.42×10^{-7}
General relativity[3]	3.69×10^{-9}	3.38×10^{-5}	1.45×10^{-12}
Albedo[1]	7.44×10^{-2}	7.22×10^{-2}	0

Superscripts: 1.Gauss method, 2. Lagrange method, 3.Cowell method

In conclusion, the influence of every disturbance on each orbital element is shown in Figure 12 to Figure 19 separately considering the changes in the type of orbit (A, B & C). A comprehensive analysis will aid in better understanding of these disturbances and their budgets on each orbit element.

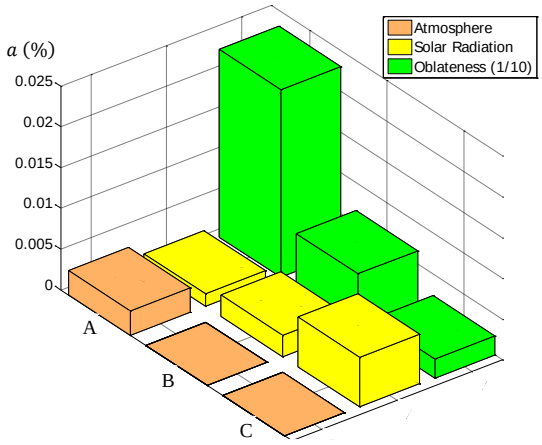

Figure 12– Orbit perturbation budgeting on **(a)** in orbit A,B & C

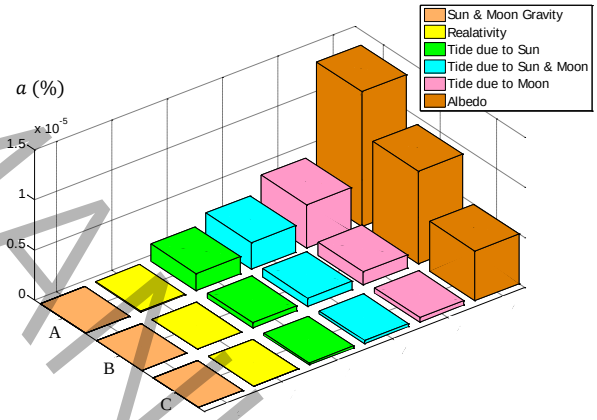

Figure 13– Orbit perturbation budgeting on **(a)** in orbit A,B & C

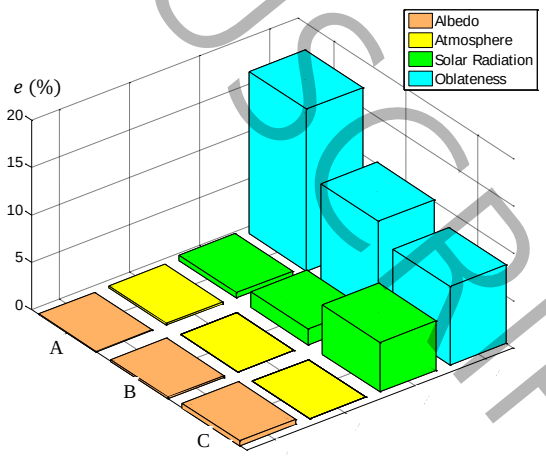

Figure 14– Orbit perturbation budgeting on ***(e)*** in orbit A,B & C

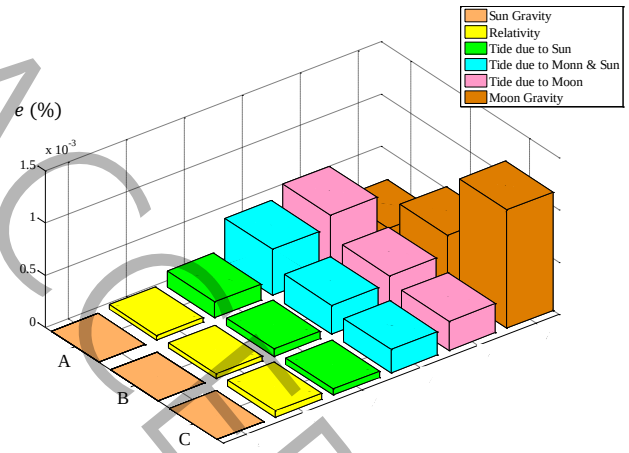

Figure 15– Orbit perturbation budgeting on ***(e)*** in orbit A,B & C

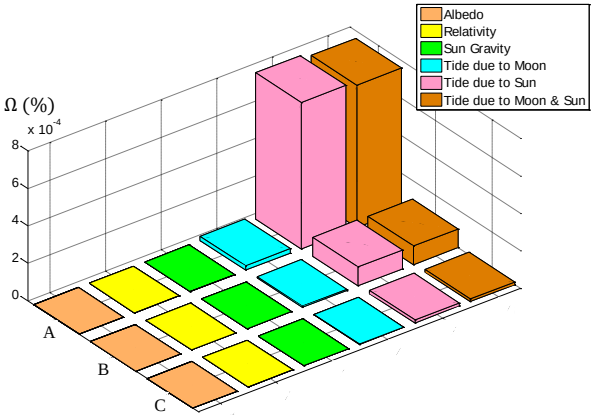

Figure 18– Orbit perturbation budgeting on (Ω) in orbit A,B & C

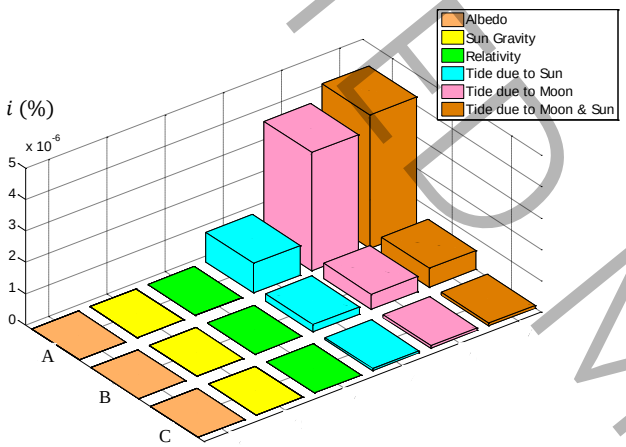

Figure 16– Orbit perturbation budgeting on (i) in orbit A,B & C

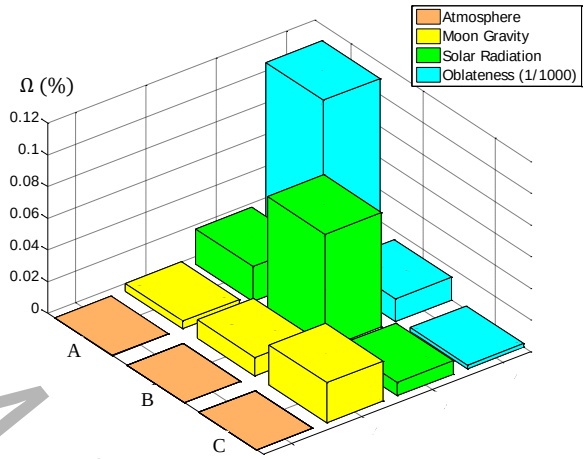

Figure 19– Orbit perturbation budgeting on ***(Ω)*** in orbit A,B & C

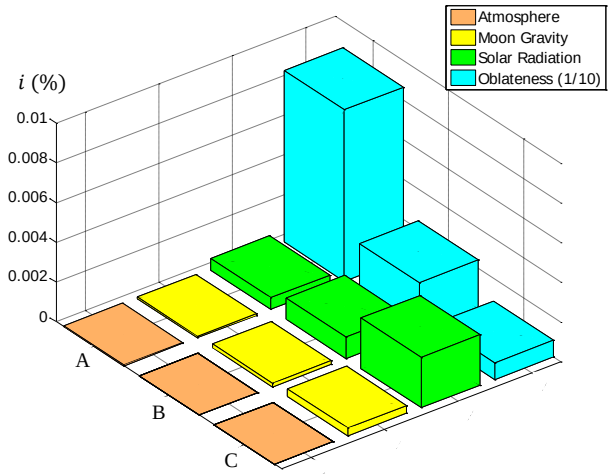

Figure 17– Orbit perturbation budgeting on (i) in orbit A,B & C

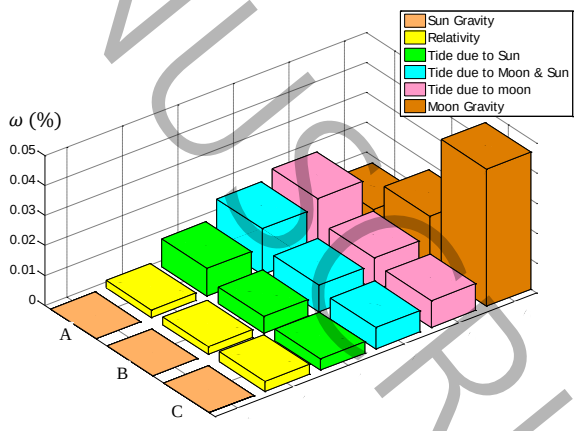

Figure 20– Orbit perturbation budgeting on ***(ω)*** in orbit A,B & C

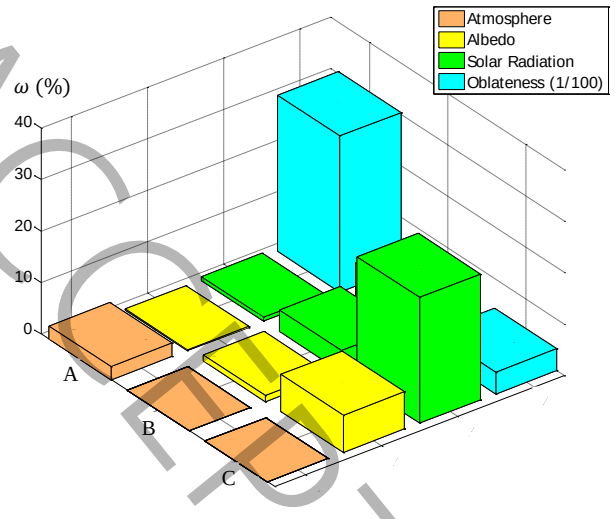

Figure 21– Orbit perturbation budgeting on ***(ω)*** in orbit A,B & C

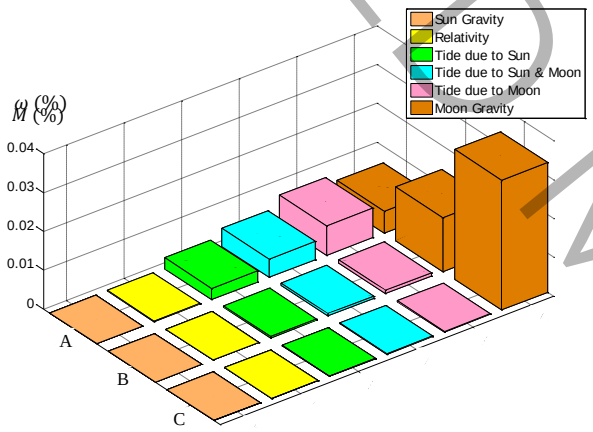

Figure 22– Orbit perturbation budgeting on ***(M)*** in orbit A,B & C

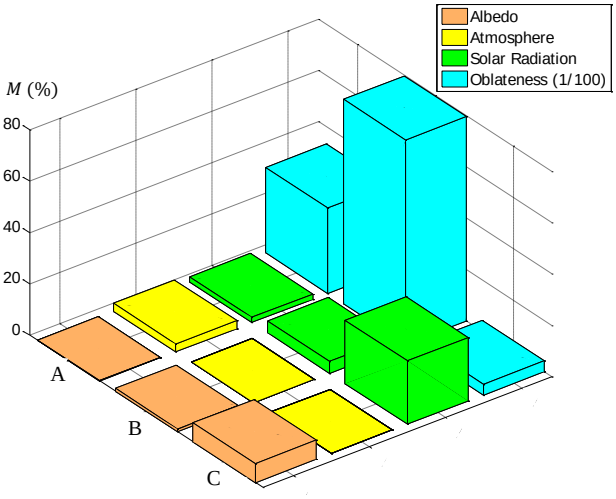

Figure 23– Orbit perturbation budgeting on ***(M)*** in orbit A,B & C

12. Conclusions

This study presents a comprehensive analysis of orbital perturbation effects across different altitude regimes, providing significant insights for spacecraft mission design and control. Our investigation reveals that Earth's oblateness (J_2 effect) represents the dominant perturbation source, with its influence decreasing as orbital altitude increases. Atmospheric drag proves most significant below 600 km, remains considerable up to 1000 km, and becomes negligible beyond this threshold. In contrast, solar radiation pressure emerges as the primary perturbing force in higher orbits, particularly in GEO and beyond. While third-body gravitational effects from the Sun and Moon exhibit direct proportionality to altitude, relativistic effects and Earth solid tides demonstrate an inverse relationship with altitude.

These findings have important implications for mission design, particularly for high-precision systems such as spatial telescopes and SAR satellites. Such applications require careful, perturbation-aware design of sensor systems, control architectures, and orbital maintenance strategies. Special consideration must be given to both Nadir-pointing systems, which are vulnerable to perturbation-induced pointing errors, and repeat-ground-track orbits that require precise perturbation compensation. For electric propulsion missions, the study highlights their heightened sensitivity to minor perturbations due to low thrust-to-perturbation ratios and multi-revolution trajectory characteristics. The established perturbation hierarchy enables optimization of thruster sizing, maneuver scheduling, and fuel budgeting.

From a theoretical perspective, this work contributes three key elements: first, a validated perturbation hierarchy for mission designers; second, altitude-dependent quantitative perturbation models; and third, a perturbation-aware control system framework. Practically, the results establish new benchmarks for precision orbital mechanics that are particularly relevant to Earth observation and communication constellations, scientific missions requiring ultra-stable orbits, and future space infrastructure deployment.

Building on these findings, future research will focus on developing optimal LEO-to-GEO transfer trajectories using hybrid electric-chemical propulsion systems. This will involve implementing heuristic optimization techniques for perturbation-compensated trajectory design, multi-objective mission planning, and robust orbital control under uncertainty, with extensions to cis-lunar station-keeping and interplanetary trajectory design. The comprehensive understanding of altitude-perturbation relationships presented in this work bridges the gap between perturbation theory and mission-ready

solutions, offering both fundamental advances and deployable tools for next-generation space systems.

Nomenclature

A	Satellite Area
a	Semi-major Axis
c	Light Speed
C_D	Drag Coefficient
C_{nm}	Tesseral spherical harmonics Coefficient
C_P	Solar Radiation Pressure Coefficient
D	Drag
E	Eccentric Anomaly
e	Eccentricity
F	Solar Flux Index
f_N	Normal Force Component
f_R	Radial Force Component
f_T	Tangential Force Component
F_{SR}	Solar Radiation Force
H	Height
h	Angular Momentum
i	Inclination
M	Mean Anomaly
m	mass
n	Mean Motion
P_n^m	Legendre polynomial Coefficient
P_{SR}	Solar Radiation Pressure
R_E	Earth Radius
r	Radius
r_p	Perigee radius
S_{nm}	Sectorial spherical harmonics Coefficient
V	Velocity
W	Angular Velocity of Atmosphere
θ	True Anomaly
λ	Longitude
μ	Body Attraction Constant
ρ	Density
v	Satellite Velocity
v_p	Perigee Velocity
ϕ	Longitude
ψ	Angle Between two Body
Ω	Longitude of Ascending Node
ω	Argument of Periapsis
ω_0	Angular Speed of Earth Rotation

References

[1] T. Verhoef and R. Noomen, Satellite Decay Computation and Impact Point Prediction, Advances in Space Research, 30(20) (2002) 313–319. DOI: 10.1016/s0273-1177(02)00301-0.

[2] J. Kabeláč and L. Sehnal, Atmospheric Effects on the Dynamics of the MIMOSA Satellite, Journal of Geodesy, 76 (2003) 536–542. DOI: 10.1007/s00190-002-0275-4.

[3] C. Pardini, W. K. Tobiska, and L. Anselmo, Analysis of the Orbital Decay of Spherical Satellites Using Different Solar Flux Proxies and Atmospheric Density Models, Advances in Space Research, 37(2) (2006) 392–400. DOI: 10.1016/j.asr.2004.10.009.

[4] N. A. Saad, M. N. Ismail, and K. H. I. Khalil, Decay of Orbits due to the Drag of Rotating Oblate Atmosphere, Planetary and Space Science, 56(3) (2008) 537–541. DOI: 10.1016/j.pss.2007.11.004.

[5] C. Pardini, L. Anselmo, K. Moe, and M. M. Moe, On the secular decay of the LARES semi-major axis, Acta Astronautica, 140 (2017) 469–477. DOI: 10.1016/j.actaastro.2017.09.012.

[6] P. Kustaanheimo and E. L. Stiefel, Perturbation theory of Keplerian motion based on spinor regularization, Journal für die Reine und Angewandte Mathematik, 218 (1965) 204–219. DOI: 10.1515/crll.1965.218.204.

[7] G. Xu, Y. Xu, and J. Xu, Analytical solution of a satellite orbit disturbed by atmospheric drag, Monthly Notices of the Royal Astronomical Society, 410(1) (2011) 654–662. DOI: 10.1111/j.1365-2966.2010.17471.x.

[8] N. Ozar, S. M. H. Al-Mamury, and H. H. Selim, The Effect of Atmospheric Drag Force on the Elements of Low Earth Orbital Satellites at Minimum Solar Activity, NeuroQuantology, 19(9) (2021) 24–37. DOI: 10.14704/nq.2021.19.9.NQ21134.

[9] N. M. Harwood and G. G. Swinerd, Long periodic and secular perturbation to the orbit of a spherical satellites due to direct solar radiation pressure, Celestial Mechanics and Dynamical Astronomy, 62(1) (1995) 71–80. DOI: 10.1007/bf00692069.

[10] W. M. Kaula, Theory of Satellite Geodesy. Waltham, MA: Blaisdell Publishing Company, (1966).

[11] M. Ziebart, High Precision Analytical Solar Radiation Pressure Modeling for GNSS Spacecrafts. London, UK: University of East London, PhD Thesis (2001).

[12] Y. Bar-Sever and D. Kuang, New Empirically Derived Solar Radiation Pressure Model for Global Positioning System Satellites. Pasadena, California: Jet Propulsion Laboratory (JPL), JPL Technical Report (2004).

[13] F. Xia, Y. Shen, and Q. Zhao, Advancing the Solar Radiation Pressure Model for BeiDou-IGSO,

Remote Sensing, 14(6) (2022). DOI: 10.3390/rs14061460.
[14] J. Žižka and D. Vokrouhlický, Solar radiation pressure on (99942) Apophis, Icarus, 211(1) (2011) 511–518. DOI: 10.1016/j.icarus.2010.08.011
[15] F. Delhaise, Analytical Treatment of Air Drag and Earth Oblateness Effect Upon An Artificial Satellite, Celestial Mechanics and Dynamical Astronomy, 52(1) (1991) 58–103.
[16] N. V. Emelyanov, The acting analytical theory of artificial Earth satellites, Astronomical & Astrophysical Transactions, 1(2) (1992) 119–127. DOI: 10.1080/10556799208244526.
[17] H. H. Selim, Analytical Third Order Solution for Coupling Effects of Earth Oblateness and Direct Solar Radiation Pressure on the Motion of Artificial Satellites, International Journal of Astronomy and Astrophysics, 4(3) (2014) 530–543. DOI: 10.4236/ijaa.2014.43049
[18] A. Masoud, M. Abdelkhalik, and A. Sharaf, Construction of Frozen Orbits Using Continuous Thrust Control Theories Considering Earth Oblateness and Solar Radiation Pressure Perturbations, Astrodynamics, 2(4) (2018) 329–343. DOI: 10.1007/s42064-018-0028-7.
[19] M. K. Ammar, M. R. Amin, and M. H. M. Hassan, Visibility intervals between two artificial satellites under the action of Earth oblateness, Applied Mathematics and Nonlinear Sciences, 3(2) (2018) 353–374. DOI: 10.21042/amns.2018.2.00028.
[20] A. El-Enna, Analytical Treatment of the Earth Oblateness and Solar Radiation Pressure Effect on an Artificial Satellite, Applied Mathematics and Computation, 151(1) (2004) 121–145. DOI: 10.1016/S0096-3003(03)00339-4.
[21] Y. Kozai, Second-order analytical solution of artificial satellite theory without air drag, The Astronomical Journal, 67(7) (1962) 446. DOI: 10.1086/108898.
[22] T. P. Brito, C. C. Celestino, and R. V. Moraes, Study of the decay time of a CubeSat type satellite considering perturbations due to the Earth's oblateness and atmospheric drag, Journal of Physics: Conference Series, 641(1) (2015), 12-26. DOI: 10.1088/1742-6596/641/1/012026.
[23] I. M. Nikolkina, L. S. Ozipova, and A. V. Shatina, "The influence of the Earth's oblateness on the image motion velocity during the electro-optical survey of the planet's surface, Journal of Physics: Conference Series, 1705(1) (2020), 12008. DOI: 10.1088/1742-6596/1705/1/012008.
[24] Y. Kozai, On the effects of the sun and moon upon the motion of a close earth satellite, Smithsonian Astrophysical Observatory Special Report, 22 (1959).
[25] P. Musen, On the long-period lunisolar effect in the motion of the artificial satellite, Journal of Geophysical Research, 66(6) (1961) 1659–1665. DOI: 10.1029/jz066i006p01659.
[26] W. M. Kaula, Development of the lunar and solar disturbing functions for a close satellite, The Astronomical Journal, 67(5) (1962) 300–303. DOI: 10.1086/108729.
[27] G. E. Cook, Luni-solar perturbations of the orbit of an earth satellite, Geophysical Journal International, 6(3) (1962) 271–291. DOI: 10.1111/j.1365-246x.1962.tb00351.x.
[28] J. P. Murphy and T. L. Felsentreger, Analysis of lunar and solar effects on the motion of close earth satellites, NASA Technical Note, no. TN D-3559, (1966).
[29] Y. Kozai, A new method to compute lunisolar perturbations in satellite motions, Smithsonian Astrophysical Observatory Special Report, 349 (1973) 1–27.
[30] R. H. Estes, On the analytic lunar and solar perturbations of a near Earth satellite, Celestial Mechanics, 10(2) (1974) 253–276. DOI: 10.1007/BF01586857.
[31] M. T. Lane, On analytic modeling of lunar perturbations of artificial satellites of the earth, Celestial Mechanics and Dynamical Astronomy, 46(4) (1989) 287–305. DOI: 10.1007/BF00049314.
[32] F. B. A. Prado, Third-body perturbation in orbits around natural satellites, Journal of Guidance, Control, and Dynamics, 26(1) (2003) 33–40. DOI: 10.2514/2.5042.
[33] R. C. Domingos, R. Vilhena de Moraes, and A. F. B. A. Prado, Third-Body Perturbation in the Case of Elliptic Orbits for the Disturbing Body, Mathematical Problems in Engineering, 763654, (2008). DOI: 10.1155/2008/763654.
[34] M. Lara, J. F. San-Juan, and L. M. López, On the third-body perturbations of high-altitude orbits, Celestial Mechanics and Dynamical Astronomy, 113(4) (2012) 435–452. DOI: 10.1007/s10569-012-9433-z.
[35] C. W. T. Roscoe, S. R. Vadali, and K. T. Alfriend, Third-Body Perturbation Effects on Satellite Formations, The Journal of the Astronautical Sciences, 60(3-4) (2013) 408–433. DOI: 10.1007/s40295-015-0057-x.
[36] T. Nie, P. Gurfil, and S. Zhang, Semi-analytical model for third-body perturbations including the inclination and eccentricity of the perturbing body, Celestial Mechanics and Dynamical Astronomy, 131(6) (2019) 29. DOI: 10.1007/s10569-019-9905-5.
[37] Q. Zeng, Y. Zheng, and J. Liu, Free and forced inclinations of orbits perturbed by the third-body gravity, Celestial Mechanics and Dynamical

Astronomy, 136(2) (2024) 16. DOI:10.1007/s10569-024-10187-2.

[38] Y. Kozai, Effect of the Tidal Deformation of the Earth on the Motion of Close Earth Satellite, Publications of the Astronomical Society of Japan, 17(4) (1965) 395–402.

[39] W. M. Kaula, Tidal Friction With Latitude-Dependent Amplitude and Phase Angle, The Astronomical Journal, 74(9) (1969) 1108–1114. DOI: 10.1086/110912.

[40] L. Iorio, Earth Tides and Lense–Thirring Effect, Celestial Mechanics and Dynamical Astronomy, 79(3) (2001) 201–230. DOI:10.1023/A:1011168615758.

[41] P. Tourrenc, M. C. Angonin, and X. Ovido, Tidal Gravitational Effects in a Satellite, General Relativity and Gravitation, 36(10) (2004) 2237–225. DOI: 10.1023/B:GERG.0000046181.95611.06.

[42] V. G. Gurzadyan, A. Paolozzi, C. Bianco, and et al., On the Earth's tidal perturbations for the LARES satellite, The European Physical Journal Plus, 132(12) (2017) 548. DOI: 10.1140/epjp/i2017-11839-3.

[43] H. Lass and C. B. Solloway, On the Comparison of the Newtonian and General Relativistic Orbits of a Point Mass in an Inverse Square Law Force Field, AIAA Journal, 7(6) (1969) 1029–1031. DOI: 10.2514/3.5271

[44] A. Ghaffar, On Some Applications of Approximate Methods in Relativistic Celestial Mechanics. Washington D.C.: NASA Goddard Space Flight Center, Technical Report TR R-341, (1970).

[45] D. Robincom, General Relativity and Satellite Orbits, Celestial Mechanics, 15(1) (1977) 21–33. DOI: 10.1007/bf01229045.

[46] M. Gulklett, Relativistic Effects in GPS and LEO. Copenhagen, Denmark: The Niels Bohr Institute, University of Copenhagen, (2003).

[47] K. Sośnica, R. Zajdel, and G. Bury, General relativistic effects acting on the orbits of Galileo satellites, Celestial Mechanics and Dynamical Astronomy, 133(4) (2021) 14. DOI: 10.1007/s10569-021-10014-y.

[48] D. Vokrouhlický and P. Farinella, Diurnal Yarkovsky effect as a source of mobility of meter-sized asteroidal fragments, Astronomy and Astrophysics, 335 (1998) 1093–1100.

[49] W. F. Bottke, D. Vokrouhlický, and M. Brož, The Effect of Yarkovsky Thermal Forces on the Dynamical Evolution of Asteroids and Meteoroids, in Asteroids III, W. F. Bottke, A. Cellino, P. Paolicchi, and R. P. Binzel, Eds. Tucson: University of Arizona Press, (2002) 395–408.

[50] D. Capek and D. Vokrouhlický, Accurate model for the Yarkovsky effect, in Dynamics of Populations of Planetary Systems, Z. Knežević and A. Milani, Eds. Cambridge: Cambridge University Press, (2005) 1–6.

[51] S. N. Deo and B. S. Kushvah, Yarkovsky effect and solar radiation pressure on the orbital dynamics of the asteroid (101955) Bennu, Astronomy and Computing, 21 (2017) 64–77. DOI: 10.1016/j.ascom.2017.07.002.

[52] T. N. Sannikov, Central Field Motion with Perturbing Acceleration Varying by the Inverse Square Law: Application to the Yarkovsky Effect, Solar System Research, 55(4) (2021) 321–331. DOI: 10.1134/s1063772921040053.

[53] T. N. Sannikov, Accounting for the Yarkovsky Effect in Reference Frames Associated with the Radius Vector and Velocity Vector, Solar System Research, 56(4) (2022) 268–278. DOI: 10.1134/s1063772922070058.

[54] D. G. King-Hele, Satellite Orbits in an Atmosphere: Theory and Applications. Glasgow, UK: Blackie & Son Ltd., (1987).

[55] D. A. Vallado, Fundamentals of Astrodynamics and Applications, 2nd ed. El Segundo, CA: Microcosm Press, (2001).

[56] K. Aksnes, Short-period and long-period perturbations of a spherical satellite due to direct solar radiation, Celestial Mechanics, 13(1) (1976) 89–104. DOI: 10.1007/bf01228536.

[57] A. Ghaffar, Integration of the Relativistic Equations of Motion of an Artificial Earth Satellite. Washington D.C.: NASA Goddard Space Flight Center, Technical Report R-346, (1970).

[58] J. P. Vinti, Orbital and Celestial Mechanics, G. J. Der and N. L. Bonavito, Eds. Reston, VA: American Institute of Aeronautics and Astronautics, (1998).

[59] G. H. J. and F. L. Hoods, Applied Orbit Perturbation and Maintenance, 2nd ed. El Segundo, CA: Aerospace Press, (2005).

[60] C. Rizos and A. Stolz, Force modeling for GPS satellite orbits, in Proceedings of the First International Symposium on Precise Positioning with the Global Positioning System, Rockville, MD, (1985) 87–98.

[61] A. F. Bogorodskii, Relativistic Effects in the Motion of an Artificial Earth Satellite, Soviet Astronomy, 3(5) (1959) 857–862.

[62] H. D. Curtis, Orbital Mechanics for Engineering Students, 3rd ed. Oxford, UK: Butterworth-Heinemann, (2013).

[63] M. J. Sidi, Spacecraft Dynamics and Control: A Practical Engineering Approach. Cambridge, UK: Cambridge University Press, (1997).